



## Article

# Synthesis and Fluorescent Properties of Multi-Functionalized $C_{70}$ Derivatives of $C_{70}(OCH_3)_{10}[C(COOEt)_2]$ and $C_{70}(OCH_3)_{10}[C(COOEt)_2]_2$

Ke Luan<sup>1</sup>, Lu Wang<sup>1</sup>, Fang-Fang Xie<sup>1</sup> , Bin-Wen Chen<sup>1</sup>, Zuo-Chang Chen<sup>1</sup>, Lin-Long Deng<sup>2,\*</sup> , Su-Yuan Xie<sup>1</sup> and Lan-Sun Zheng<sup>1</sup>

<sup>1</sup> State Key Laboratory for Physical Chemistry of Solid Surfaces, Collaborative Innovation Center of Chemistry for Energy Materials, Department of Chemistry, College of Chemistry and Chemical Engineering, Xiamen University, Xiamen 361005, China; luanke9411@163.com (K.L.); 20520201151919@stu.xmu.edu.cn (L.W.); fangfangxie0707@163.com (F.-F.X.); cbw15959235525@163.com (B.-W.C.); zcchem@126.com (Z.-C.C.); syxie@xmu.edu.cn (S.-Y.X.); lszheng@xmu.edu.cn (L.-S.Z.)

<sup>2</sup> Pen-Tung Sah Institute of Micro-Nano Science and Technology, Xiamen University, Xiamen 361005, China

\* Correspondence: denglinlong@xmu.edu.cn

**Abstract:** Due to the partially reduced  $\pi$ -conjugation of the fullerene cage, multi-functionalized fullerene derivatives exhibit remarkable fluorescent properties compared to pristine fullerenes, which have high potential for application in organic light-emitting diodes (OLEDs). In this study two multi-functionalized  $C_{70}$  derivatives,  $C_{70}(OCH_3)_{10}[C(COOEt)_2]$  and  $C_{70}(OCH_3)_{10}[C(COOEt)_2]_2$ , with excellent fluorescence properties, were designed and synthesized. Compared with  $C_{70}(OCH_3)_{10}$  containing a single kind of functional group, both the  $C_{70}(OCH_3)_{10}[C(COOEt)_2]$  and  $C_{70}(OCH_3)_{10}[C(COOEt)_2]_2$  exhibited enhanced fluorescence properties with blue fluorescence emission. The fluorescence quantum yields of the  $C_{70}(OCH_3)_{10}[C(COOEt)_2]$  and  $C_{70}(OCH_3)_{10}[C(COOEt)_2]_2$  were 1.94% and 2.30%, respectively, which were about ten times higher than that of  $C_{70}(OCH_3)_{10}$ . The theoretical calculations revealed that the multi-functionalization of the  $C_{70}$  increased the  $S_1-T_1$  energy gap, reducing the intersystem crossing efficiency, resulting in the higher fluorescence quantum yield of the  $C_{70}$  derivatives. The results indicate that multi-functionalization is a viable strategy to improve the fluorescence of fullerene derivatives.

**Keywords:** fullerene; multi-functionalization; fluorescence



**Citation:** Luan, K.; Wang, L.; Xie, F.-F.; Chen, B.-W.; Chen, Z.-C.; Deng, L.-L.; Xie, S.-Y.; Zheng, L.-S. Synthesis and Fluorescent Properties of Multi-Functionalized  $C_{70}$  Derivatives of  $C_{70}(OCH_3)_{10}[C(COOEt)_2]$  and  $C_{70}(OCH_3)_{10}[C(COOEt)_2]_2$ . *Nanomaterials* **2022**, *12*, 1426. <https://doi.org/10.3390/nano12091426>

Academic Editor: Mohammed Jaouad Meziani

Received: 29 March 2022

Accepted: 20 April 2022

Published: 22 April 2022

**Publisher's Note:** MDPI stays neutral with regard to jurisdictional claims in published maps and institutional affiliations.



**Copyright:** © 2022 by the authors. Licensee MDPI, Basel, Switzerland. This article is an open access article distributed under the terms and conditions of the Creative Commons Attribution (CC BY) license (<https://creativecommons.org/licenses/by/4.0/>).

## 1. Introduction

Fluorescence studies on fullerenes and their derivatives have attracted great interest from researchers [1–13], who can not only offer vital information on the excited electronic structures of fullerenes and their derivatives, but can also assess their potential applications in organic electronic devices [14,15]. Due to the renowned electron-accepting ability and small reorganization energy of symmetric fullerenes [16,17], the transition from  $S_0$  to  $S_1$  is forbidden, and the intersystem crossing (ISC) efficiency from  $S_1$  to  $T_1$  is very high (close to 100%) [18]. Pristine fullerenes exhibit poor fluorescence properties, such as low-fluorescence quantum yields ( $\Phi$  of ca. 0.03% for  $C_{60}$  and ca. 0.06% for  $C_{70}$  in toluene) and short fluorescence lifetimes ( $\tau$  of 1.2 ns for  $C_{60}$  and 0.67 ns for  $C_{70}$ ) [19–22]. The functionalization of fullerene is a valid way to increase electronic transition forbiddance and the  $S_1-T_1$  energy gap by lowering the symmetry of the fullerene. However, the fluorescence of mono-, bis-, and tris-adducts of fullerene derivatives is still extremely weak, since these adducts cannot effectively destroy the symmetric structure of fullerenes [23]. Multi-functionalization with higher adducts has been proven to be an effective methodology to fine-tune the fluorescence properties of fullerene derivatives. For instance, Rubin et al. reported a hexa-adduct of  $C_{60}$  that exhibited much-improved fluorescence intensity [24]. Multi-functionalized  $C_{60}$  derivatives with excellent

fluorescence properties were prepared by Nakamura et al. [25–27]. Compared with the studies on the fluorescence properties of  $C_{60}$  derivatives, there are few studies on the fluorescence properties of  $C_{70}$  derivatives [28].

Herein, we report the synthesis and fluorescence properties of two multi-functionalized  $C_{70}$  derivatives,  $C_{70}(\text{OCH}_3)_{10}[\text{C}(\text{COOEt})_2]$  and  $C_{70}(\text{OCH}_3)_{10}[\text{C}(\text{COOEt})_2]_2$ . By carefully controlling the molar ratio of the reactants,  $C_{70}(\text{OCH}_3)_{10}[\text{C}(\text{COOEt})_2]$  and  $C_{70}(\text{OCH}_3)_{10}[\text{C}(\text{COOEt})_2]_2$  can be readily synthesized from  $C_{70}(\text{OCH}_3)_{10}$  by using the Bingel–Hirsch reaction with high selectivity. Due to the reduced  $\pi$ -conjugated system of  $C_{70}$ , the fluorescence quantum yield of  $C_{70}(\text{OCH}_3)_{10}[\text{C}(\text{COOEt})_2]$  and  $C_{70}(\text{OCH}_3)_{10}[\text{C}(\text{COOEt})_2]_2$  was about ten times higher than that of  $C_{70}(\text{OCH}_3)_{10}$ . The results provide a method for synthesizing fullerene derivatives with excellent fluorescence, offering valuable materials for organic light-emitting diodes.

## 2. Materials and Methods

### 2.1. Materials and Synthesis

$C_{70}$ , iodine monochloride (ICl), silver perchlorate, diethyl bromomalonate, and 1,8-diazabicyclo[5.4.0]undec-7-ene (DBU) were purchased from commercial suppliers and used as received without further purification. Solvents were distilled and dried by standard procedures.

$C_{70}\text{Cl}_{10}$  and  $C_{70}(\text{OCH}_3)_{10}$  were prepared according to the procedure in the literature [28,29].

$C_{70}(\text{OCH}_3)_{10}[\text{C}(\text{COOEt})_2]$ : Diethyl bromomalonate (12 mg, 0.05 mmol) and DBU (16 mg, 0.1 mmol) were added to a solution of  $C_{70}(\text{OCH}_3)_{10}$  (58 mg, 0.05 mmol) in anhydrous toluene (50 mL). The mixture was stirred overnight under atmosphere at room temperature. The solvent was removed under reduced pressure and the crude product was purified by column chromatography over silica gel with toluene/acetate (10:1) as the eluents to produce  $C_{70}(\text{OCH}_3)_{10}[\text{C}(\text{COOEt})_2]$  as a pale-yellow solid (22 mg, 33%).  $^1\text{H}$  NMR (500 MHz,  $\text{CDCl}_3$ , ppm):  $\delta$  4.21 (q,  $J = 7.0$  Hz, 4H), 3.98 (s, 6H), 3.93 (s, 12H), 3.86 (s, 6H), 3.75 (s, 6H), and 1.22 (t,  $J = 7.0$  Hz, 6H).  $^{13}\text{C}$  NMR (500 MHz,  $\text{CDCl}_3$ , ppm):  $\delta$  163.56, 153.40, 153.07, 151.78, 151.29, 150.78, 150.73, 149.91, 149.40, 148.90, 148.54, 148.42, 148.24, 148.22, 148.11, 147.88, 147.79, 146.61, 146.49, 146.13, 145.41, 145.12, 143.71, 142.96, 139.00, 138.83, 138.58, 137.46, 135.93, 134.20, 129.04, 128.23, 86.18, 81.21, 81.03, 80.81, 80.69, 67.79, 65.89, 63.10, 56.18, 56.11, 55.94, 55.91, 55.85, 43.47, and 14.03. ESI-FT-ICR-HRMS  $\text{C}_{87}\text{H}_{40}\text{O}_{14} [\text{M}+\text{Na}]^+$   $m/z$  calculated 1331.2310 found 1331.2311.

The  $C_{70}(\text{OCH}_3)_{10}[\text{C}(\text{COOEt})_2]_2$ : Diethyl bromomalonate (48 mg, 0.2 mmol) and DBU (60 mg, 0.4 mmol) were added to a solution of  $C_{70}(\text{OCH}_3)_{10}$  (58 mg, 0.05 mmol) in anhydrous toluene (50 mL). The mixture was stirred overnight under atmosphere at room temperature. The solvent was removed under reduced pressure and the crude product was purified by column chromatography over silica gel with toluene/acetate (5:1) as the eluents to afford  $C_{70}(\text{OCH}_3)_{10}[\text{C}(\text{COOEt})_2]_2$  as a light-yellow solid (29 mg, 39%).  $^1\text{H}$  NMR (500 MHz,  $\text{CDCl}_3$ , ppm):  $\delta$  4.33 (m, 8H), 4.00–3.77 (m, 30H), and 1.38–1.30 (m, 12H).  $^{13}\text{C}$  NMR (500 MHz,  $\text{CDCl}_3$ , ppm):  $\delta$  163.70, 163.67, 163.64, 163.21, 154.21, 153.22, 151.89, 151.80, 151.39, 151.34, 150.58, 150.33, 150.00, 149.62, 149.02, 148.90, 148.59, 148.31, 147.83, 147.53, 147.24, 146.91, 146.62, 146.52, 146.44, 146.30, 145.85, 145.60, 145.30, 145.26, 145.01, 144.60, 144.47, 143.67, 142.71, 139.95, 139.66, 139.12, 138.89, 138.14, 137.77, 137.52, 136.59, 136.24, 135.58, 134.38, 133.50, 130.01, 85.49, 84.51, 81.06, 80.94, 80.86, 80.80, 80.76, 80.70, 67.89, 67.80, 63.10, 63.07, 62.94, 62.88, 55.97, 55.93, 55.87, 55.79, 55.71, 55.68, 55.20, 43.44, 41.00, and 14.06. ESI-FT-ICR-HRMS  $\text{C}_{94}\text{H}_{50}\text{O}_{18} [\text{M}+\text{Na}]^+$   $m/z$  calculated 1490.3847 found 1490.2916.

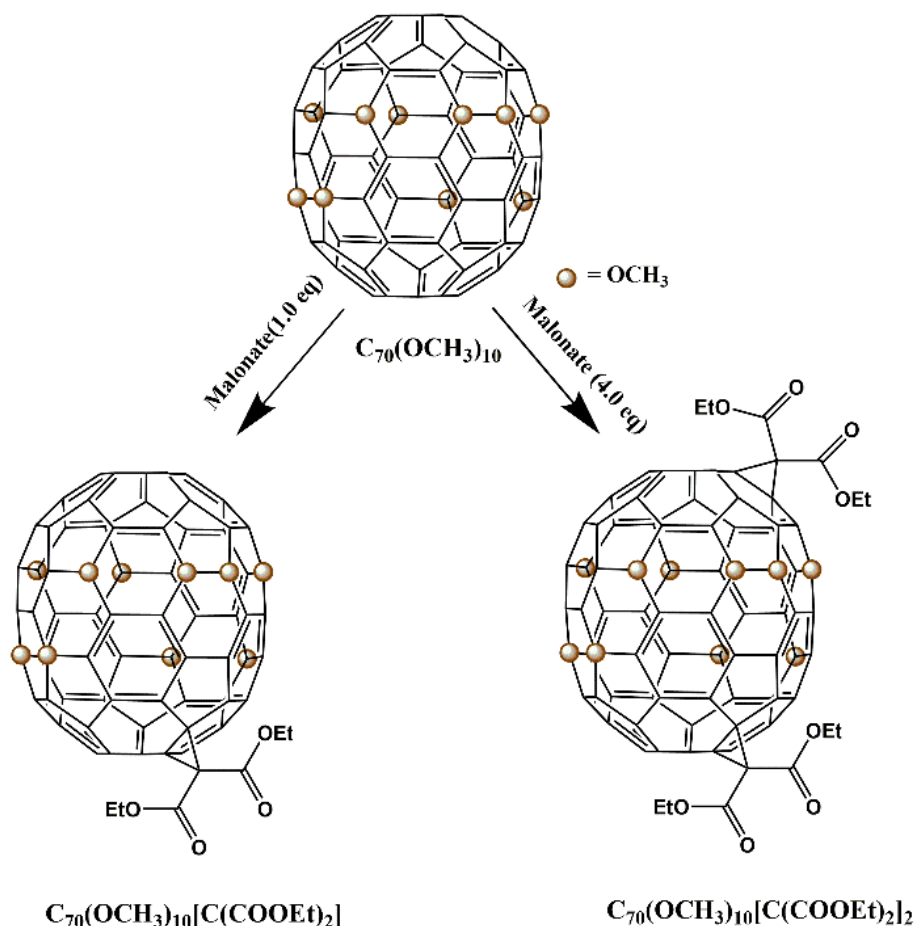
### 2.2. Characterization

$^1\text{H}$  NMR,  $^{13}\text{C}$  NMR, and 2D NMR spectra were recorded using Bruker AVIII500 spectrometers (Bruker, Billerica, MA, USA). High-resolution mass spectra (HRMS) were recorded on Agilent G6545XT mass spectrometers (Agilent, Santa Clara, CA, USA). UV-vis absorption spectra in solution were recorded using an Agilent Cary 5000 spectrophotometer (Agilent, Santa Clara, CA, USA). The spectra were measured in quartz glass cuvettes using spectroscopic grade solvents. Fluorescence spectroscopy in solution was carried out

with an FLS980 spectrometer (Edinburgh Instruments, Livingston, UK). Time-resolved measurements were performed with a PS laser diode and a TCSPC detection unit. Single-crystal X-ray data were collected on a Rigaku Xtalab Synergy diffractometer (Rigaku, Tokyo, Japan). Using Olex2 [30], the initial structure was solved with the SHELX-XT structure solution program using direct method and refined with the XL refinement package using least-squares minimization.

### 3. Results and Discussion

As shown in Scheme 1, the  $C_{70}(OCH_3)_{10}[C(COOEt)_2]$  and  $C_{70}(OCH_3)_{10}[C(COOEt)_2]_2$  were synthesized from  $C_{70}(OCH_3)_{10}$  by Bingel–Hirsch reaction. The deca-adduct  $C_{70}(OCH_3)_{10}$  was readily prepared by treating the  $C_{70}Cl_{10}$  with anhydrous methanol in the presence of silver perchlorate.  $C_{70}(OCH_3)_{10}[C(COOEt)_2]$  and  $C_{70}(OCH_3)_{10}[C(COOEt)_2]_2$  can be readily synthesized with high selectivity by carefully controlling the molar ratio of the reactants. Their molecular structures were confirmed by  $^1H$ ,  $^{13}C$  NMR spectroscopy and high-resolution mass spectrometry (Figures S1–S10). The two-dimensional correlated spectroscopy (COSY) showed that there was mutual coupling of the protons between the methyl and the methylene in the ethyl malonate of both the  $C_{70}(OCH_3)_{10}[C(COOEt)_2]$  and the  $C_{70}(OCH_3)_{10}[C(COOEt)_2]_2$  molecules (Figures S4 and S9).



**Scheme 1.** Synthesis of  $C_{70}(OCH_3)_{10}[C(COOEt)_2]$  and  $C_{70}(OCH_3)_{10}[C(COOEt)_2]_2$ .

The structure of the  $C_{70}(OCH_3)_{10}[C(COOEt)_2]$  was unambiguously determined by X-ray crystallographic analysis (Figure 1 and Table S1). Single crystals were obtained through the slow diffusion of hexane into a toluene solution of  $C_{70}(OCH_3)_{10}[C(COOEt)_2]$ . As shown in Figure 1, all the methoxy groups were distributed on the equatorial region of the  $C_{70}$  cage. The malonate group was added to the pole of the  $C_{70}$  cage, and the

ester groups were pointed in different directions to minimize the steric hindrance. In the crystalline state, the  $C_{70}(OCH_3)_{10}[C(COOEt)_2]$  molecules displayed ordered packing in all the directions of the a-, b- and c-axes. Although the single crystal of the  $C_{70}(OCH_3)_{10}[C(COOEt)_2]_2$  was not obtained, the most favorable structure of  $C_{70}(OCH_3)_{10}[C(COOEt)_2]_2$  was determined through a series of theoretical calculations (Figures S11–S13). As shown in Figure S14, the two malonate groups were distributed at the two poles of the  $C_{70}$  cage. Similarly, all the functionalized groups were oriented in different directions to minimize the steric hindrance.

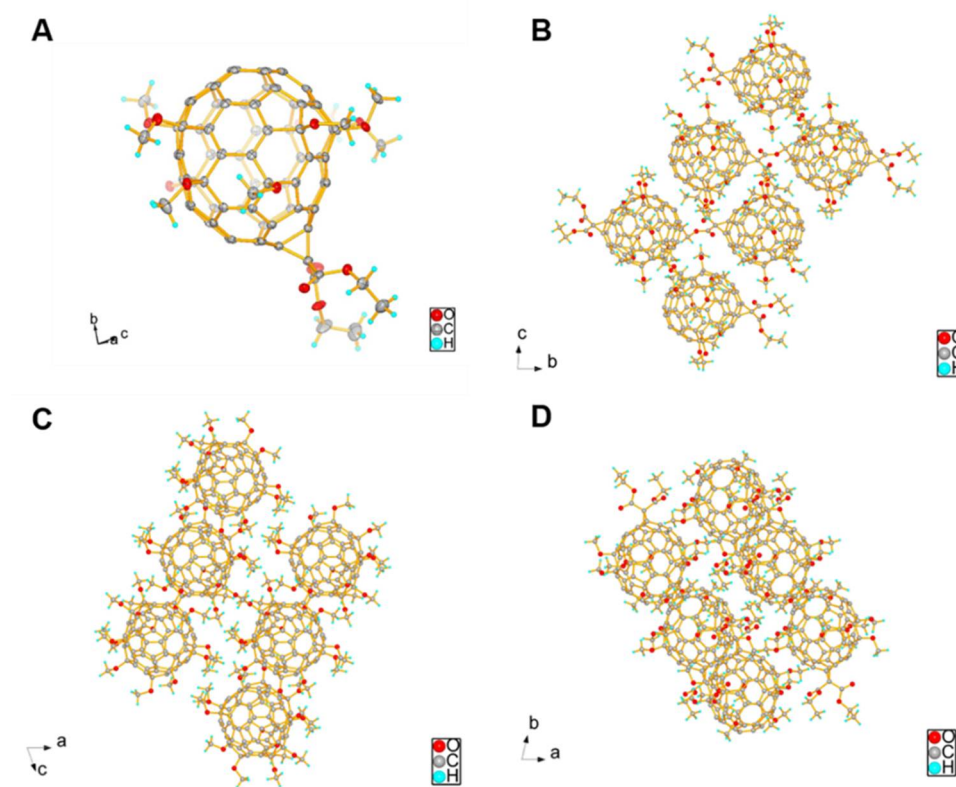


**Figure 1.** Crystal structure of  $C_{70}(OCH_3)_{10}[C(COOEt)_2]$ . (A) ORTEP drawing with 50% ellipsoid probability. The molecular packing along a-axis (B), b-axis (C), and c-axis (D).

The UV-vis absorption spectra of the  $C_{70}(OCH_3)_{10}$ ,  $C_{70}(OCH_3)_{10}[C(COOEt)_2]$ , and  $C_{70}(OCH_3)_{10}[C(COOEt)_2]_2$  were measured at room temperature. As shown in Figure 2, the  $C_{70}(OCH_3)_{10}$  exhibited two absorption peaks at 435 and 480 nm in the visible region, and one absorption peak at 315 nm in the ultraviolet region. By contrast, there was no absorption peak in the visible region, but there was one absorption peak in the ultraviolet region (313 nm) for  $C_{70}(OCH_3)_{10}[C(COOEt)_2]$ , which was slightly blue-shifted with respect to the  $C_{70}(OCH_3)_{10}$ . Similarly, the  $C_{70}(OCH_3)_{10}[C(COOEt)_2]_2$  showed an absorption peak at 305 nm, which was further blue-shifted compared with that of the  $C_{70}(OCH_3)_{10}[C(COOEt)_2]$ . Moreover, a broad shoulder peak around 370 nm was observed for the  $C_{70}(OCH_3)_{10}[C(COOEt)_2]$ . The blue-shifting of the absorption peaks of both  $C_{70}(OCH_3)_{10}[C(COOEt)_2]$  and  $C_{70}(OCH_3)_{10}[C(COOEt)_2]_2$  was caused by the decrease in the  $\pi$ -conjugated system of the  $C_{70}$  cage, indicating that the energy gap between the  $S_1$  and  $S_0$  became larger.

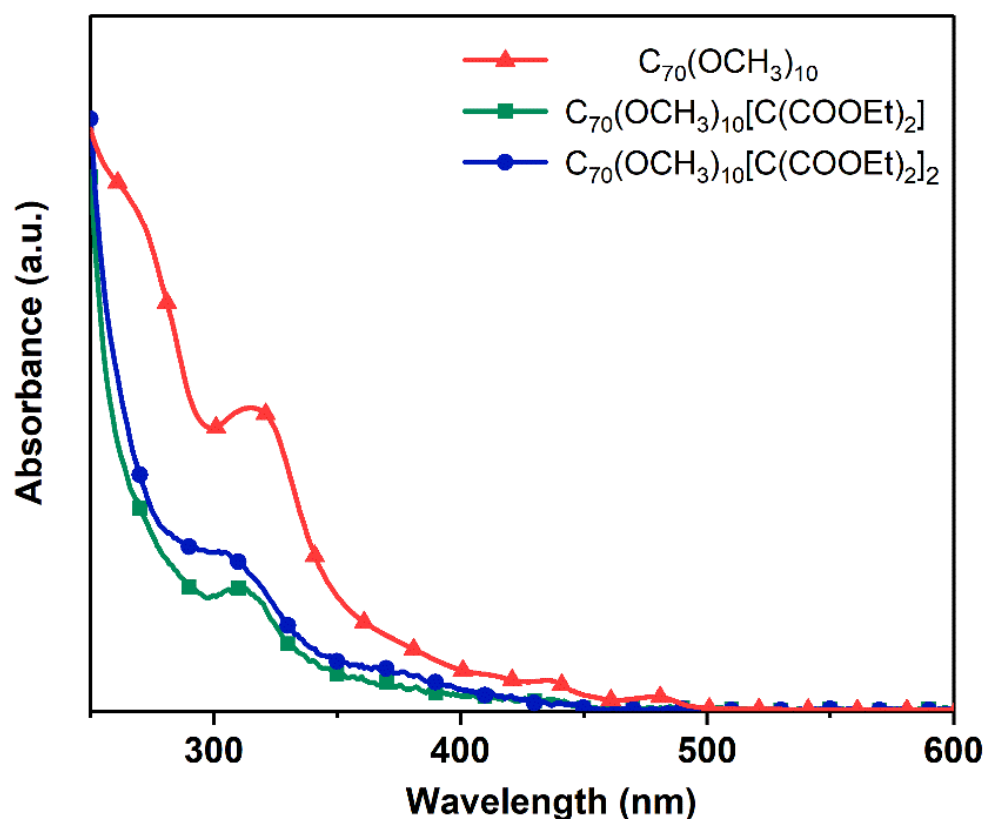


**Figure 2.** UV-vis absorption spectra of C<sub>70</sub>(OCH<sub>3</sub>)<sub>10</sub>, C<sub>70</sub>(OCH<sub>3</sub>)<sub>10</sub>[C(COOEt)<sub>2</sub>], and C<sub>70</sub>(OCH<sub>3</sub>)<sub>10</sub>[C(COOEt)<sub>2</sub>]<sub>2</sub> in a 1.0 × 10<sup>−5</sup> mol/L chloroform solution at room temperature.

To obtain information about the photophysical properties of the C<sub>70</sub>(OCH<sub>3</sub>)<sub>10</sub>, C<sub>70</sub>(OCH<sub>3</sub>)<sub>10</sub>[C(COOEt)<sub>2</sub>], and C<sub>70</sub>(OCH<sub>3</sub>)<sub>10</sub>[C(COOEt)<sub>2</sub>]<sub>2</sub>, we measured the steady-state fluorescence spectra of these C<sub>70</sub> derivatives. As shown in Figure 3, the emission peak of the C<sub>70</sub>(OCH<sub>3</sub>)<sub>10</sub> was 498 nm, with a shoulder peak at 521 nm. The major emission peak at 498 nm was ascribed to the S<sub>1</sub>→S<sub>0</sub> transition, and the shoulder peak was ascribed to the transition involving the vibronic interactions [4,5]. The fluorescence spectra of the C<sub>70</sub>(OCH<sub>3</sub>)<sub>10</sub>[C(COOEt)<sub>2</sub>] and C<sub>70</sub>(OCH<sub>3</sub>)<sub>10</sub>[C(COOEt)<sub>2</sub>]<sub>2</sub> were rather similar. The major peaks appeared at 451 and 454 nm for the C<sub>70</sub>(OCH<sub>3</sub>)<sub>10</sub>[C(COOEt)<sub>2</sub>] and the C<sub>70</sub>(OCH<sub>3</sub>)<sub>10</sub>[C(COOEt)<sub>2</sub>]<sub>2</sub>, respectively, while the shoulder peaks were shown at 480, and 481 nm. Obviously, the fluorescence emission peaks of the C<sub>70</sub>(OCH<sub>3</sub>)<sub>10</sub>[C(COOEt)<sub>2</sub>] and C<sub>70</sub>(OCH<sub>3</sub>)<sub>10</sub>[C(COOEt)<sub>2</sub>]<sub>2</sub> were blue-shifted compared to those of the C<sub>70</sub>(OCH<sub>3</sub>)<sub>10</sub>, indicating that the Bingel–Hirsch reaction can effectively reduce the π-conjugated system of the C<sub>70</sub> cage [21]. The fluorescence quantum yields of these fullerene derivatives were obtained with integrating spheres. The fluorescence quantum yields of the C<sub>70</sub>(OCH<sub>3</sub>)<sub>10</sub>[C(COOEt)<sub>2</sub>] and C<sub>70</sub>(OCH<sub>3</sub>)<sub>10</sub>[C(COOEt)<sub>2</sub>]<sub>2</sub> were 1.94, and 2.30%, respectively, which were about ten times higher than that of the C<sub>70</sub>(OCH<sub>3</sub>)<sub>10</sub> (0.25%). However, the fluorescence quantum yields of both the C<sub>70</sub>(OCH<sub>3</sub>)<sub>10</sub>[C(COOEt)<sub>2</sub>] and the C<sub>70</sub>(OCH<sub>3</sub>)<sub>10</sub>[C(COOEt)<sub>2</sub>]<sub>2</sub> were not particularly high, which made them difficult to use as fluorescent labels.

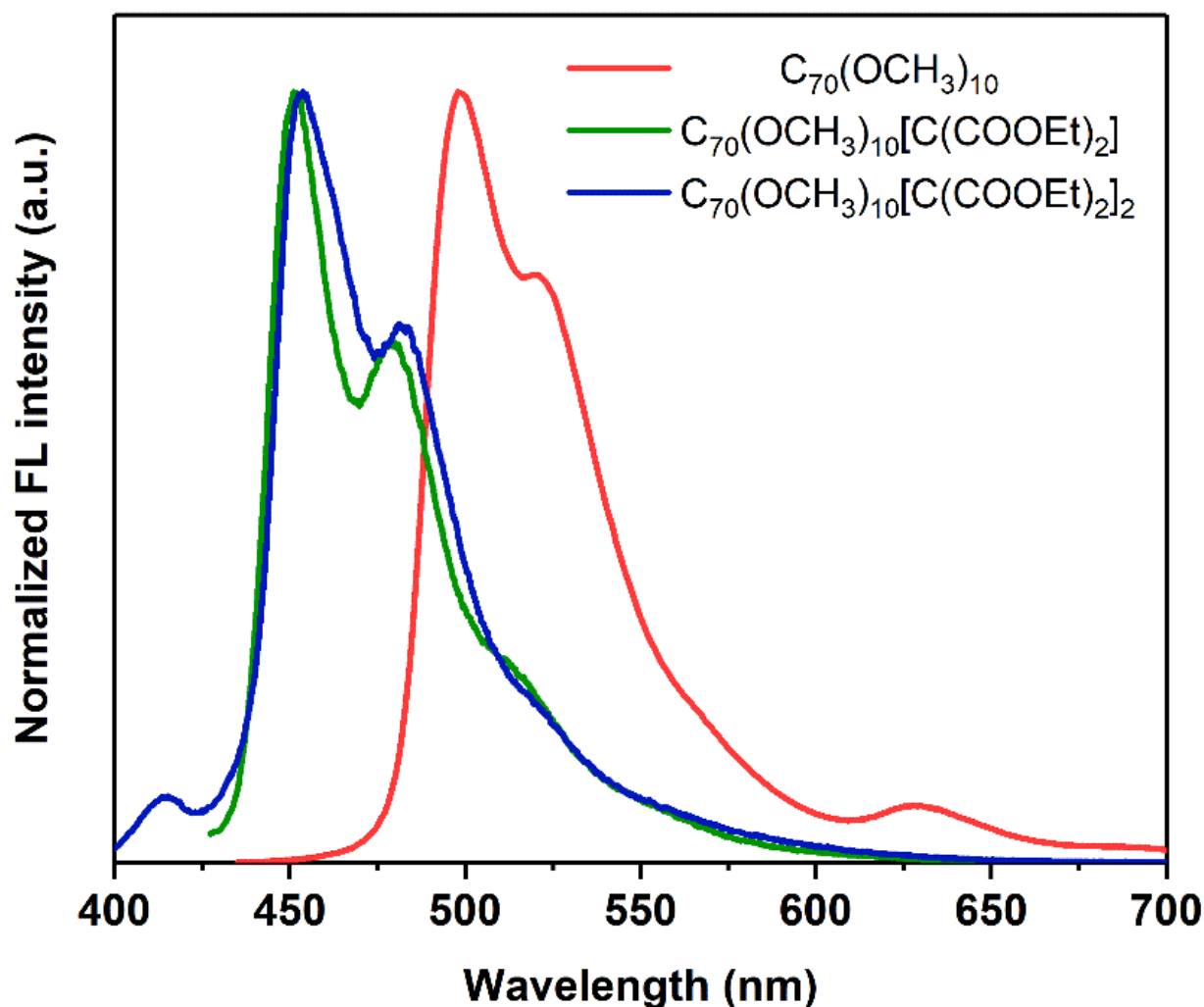


**Figure 3.** Normalized steady-state fluorescence spectra of  $C_{70}(OCH_3)_{10}$ ,  $C_{70}(OCH_3)_{10}[C(COOEt)_2]$ , and  $C_{70}(OCH_3)_{10}[C(COOEt)_2]_2$  at room temperature.

The fluorescent decay profiles of the  $C_{70}(OCH_3)_{10}$ ,  $C_{70}(OCH_3)_{10}[C(COOEt)_2]$ , and  $C_{70}(OCH_3)_{10}[C(COOEt)_2]_2$  in chloroform were recorded using the time-correlated single-photon counting (TCSPC) method. The fluorescence lifetime of the  $C_{70}(OCH_3)_{10}$  was described by a single-exponential component with  $\tau = 1.16$  ns. However, the fluorescence lifetime of the  $C_{70}(OCH_3)_{10}[C(COOEt)_2]$  ( $\tau = 1.99$  ns) was described by double-exponential components with  $\tau_1 = 1.18$  ns (70.9%) and  $\tau_2 = 3.95$  ns (29.1%). Similarly, the fluorescence lifetime of the  $C_{70}(OCH_3)_{10}[C(COOEt)_2]_2$  ( $\tau = 1.82$  ns) was also described by bi-exponential components with  $\tau_1 = 1.18$  ns (72.0%) and  $\tau_2 = 3.44$  ns (28.0%) (Table 1). As shown in Figure 4, the fluorescence lifetimes of the  $C_{70}(OCH_3)_{10}[C(COOEt)_2]$  and  $C_{70}(OCH_3)_{10}[C(COOEt)_2]_2$  were slightly longer than those of the  $C_{70}(OCH_3)_{10}$ , which implies that the number of adducts on fullerene can influence the fluorescence lifetime of fullerene derivatives [27]. Fullerene derivatives with more adducts may have higher fluorescence quantum yields and longer fluorescence lifetimes. Therefore, multi-functionalization is a promising strategy to improve the fluorescence of fullerene derivatives.

**Table 1.** Fluorescence lifetimes of  $C_{70}(OCH_3)_{10}$ ,  $C_{70}(OCH_3)_{10}[C(COOEt)_2]$  and  $C_{70}(OCH_3)_{10}[C(COOEt)_2]_2$ . The values in parentheses represent the fractions of each kinetic lifetime.

	$\tau_1$ (ns)	$\tau_2$ (ns)	$\tau$ (ns)	QY (%)
$C_{70}(OCH_3)_{10}$	1.16 (100%)		1.16	0.25
$C_{70}(OCH_3)_{10}[C(COOEt)_2]$	1.18 (70.9%)	3.95 (29.1%)	1.99	1.94
$C_{70}(OCH_3)_{10}[C(COOEt)_2]_2$	1.18 (72.0%)	3.44 (28.0%)	1.82	2.30

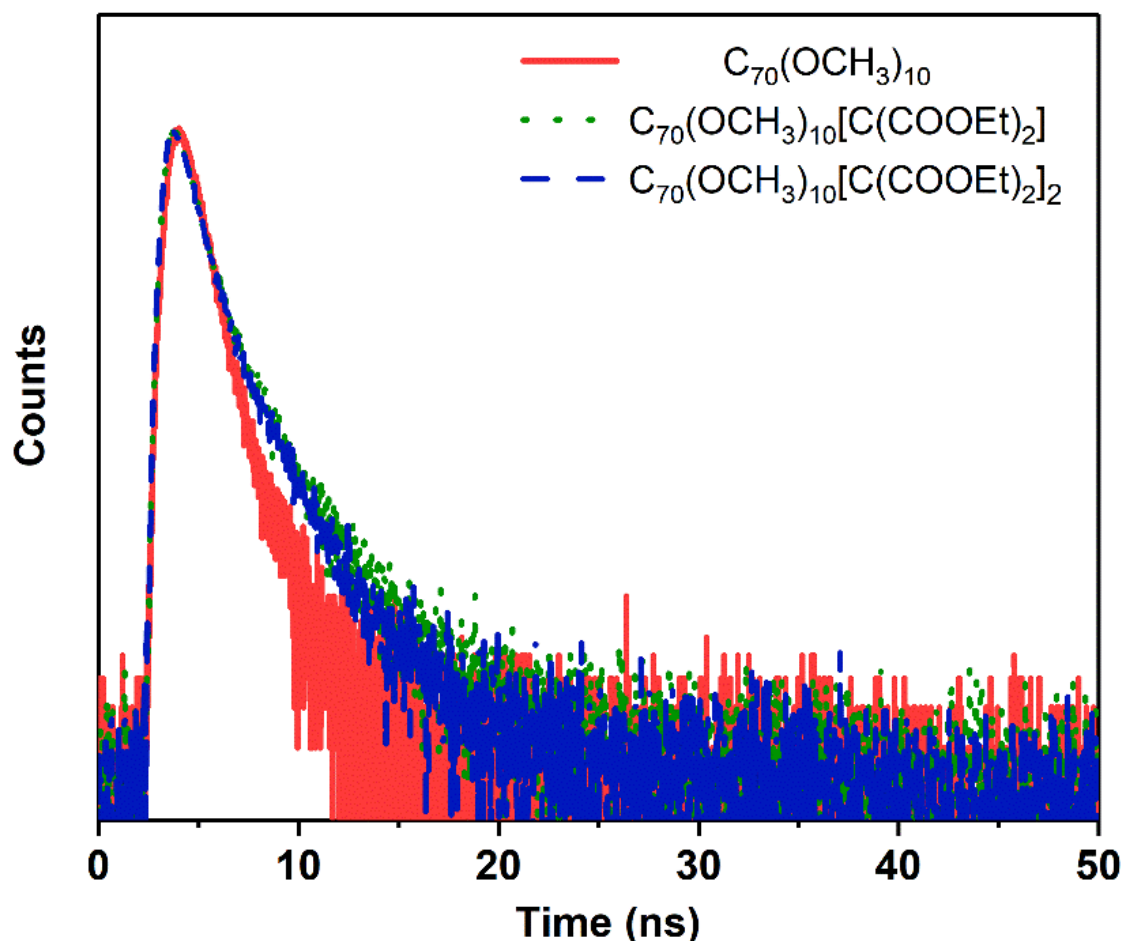


**Figure 4.** Time-resolved fluorescence decay profiles of  $C_{70}(OCH_3)_{10}$ ,  $C_{70}(OCH_3)_{10}[C(COOEt)_2]$ , and  $C_{70}(OCH_3)_{10}[C(COOEt)_2]_2$ .

To gain insight into the mechanisms of the fluorescence enhancements, we carried out theoretical calculations. Generally, the compounds with high fluorescence quantum yields had large  $S_1-T_1$  energy gaps. Furthermore, the larger  $S_1-T_1$  energy gaps appeared when the excitation was more localized. As shown in Figure 5, the difference  $S_1/S_0$  electronic densities of the  $C_{70}(OCH_3)_{10}$ ,  $C_{70}(OCH_3)_{10}[C(COOEt)_2]$ , and  $C_{70}(OCH_3)_{10}[C(COOEt)_2]_2$  were computed through TD-DFT. The excitations of the  $C_{70}(OCH_3)_{10}[C(COOEt)_2]$  and  $C_{70}(OCH_3)_{10}[C(COOEt)_2]_2$  were similar and spatially localized in the same fragment of the molecule, which meant a large  $S_1-T_1$  energy gap. However, the large spatial extension led to a small  $S_1-T_1$  energy gap, as with the  $C_{70}(OCH_3)_{10}$ . Therefore, the further functionalization of the  $C_{70}(OCH_3)_{10}$  increased the  $S_1-T_1$  energy gap, reducing the intersystem crossing efficiency, resulting in the higher fluorescence quantum yield of the  $C_{70}$  derivatives.

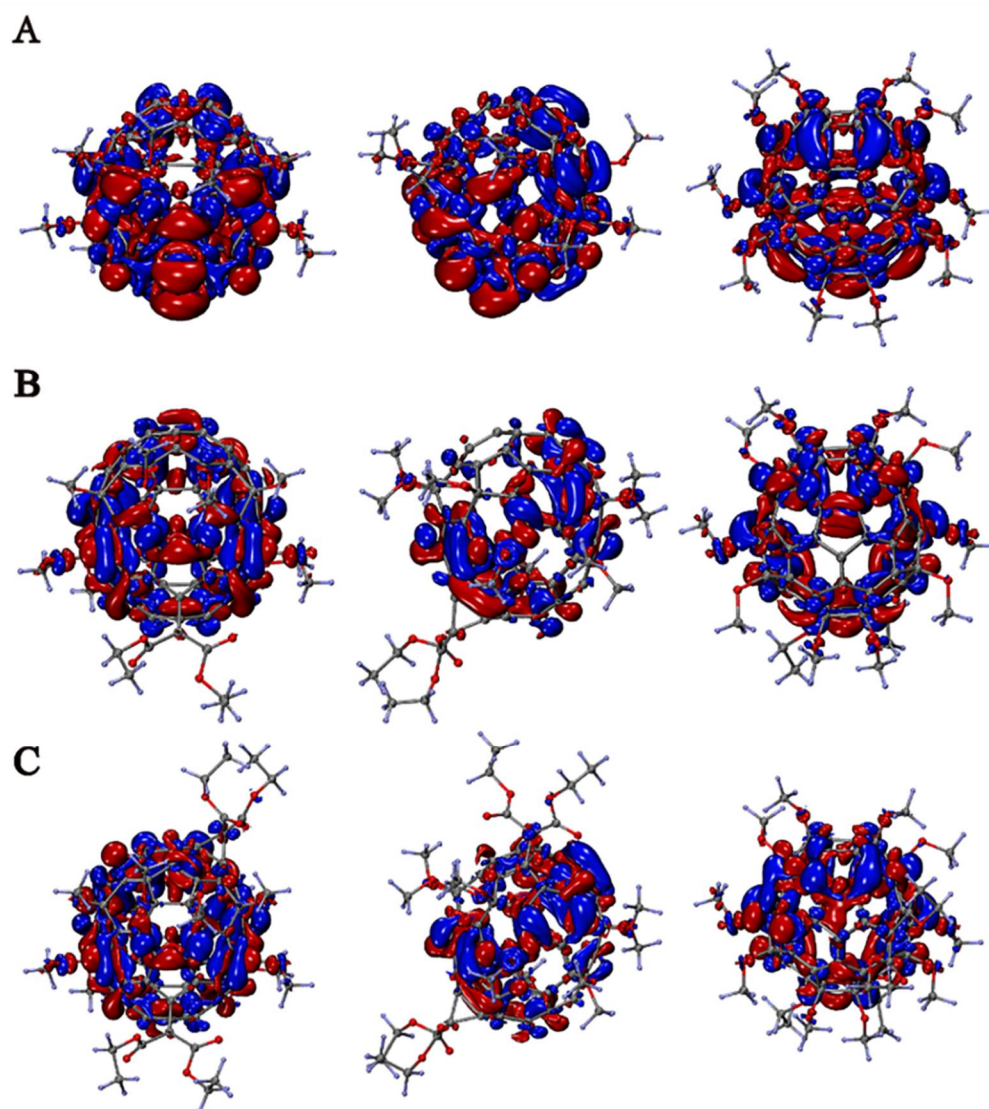


**Figure 5.** TD-DFT computed difference  $S_1/S_0$  electronic densities of  $C_{70}(OCH_3)_{10}$  (A),  $C_{70}(OCH_3)_{10}[C(COOEt)_2]$  (B), and  $C_{70}(OCH_3)_{10}[C(COOEt)_2]_2$  (C). Positive and negative parts are red and blue, respectively. Each molecule is shown in three orientations: front view, side view, and top view.

#### 4. Conclusions

In summary, two multi-functionalized  $C_{70}$  derivatives,  $C_{70}(OCH_3)_{10}[C(COOEt)_2]$  and  $C_{70}(OCH_3)_{10}[C(COOEt)_2]_2$ , were synthesized from  $C_{70}(OCH_3)_{10}$  by Bingel–Hirsch reaction with high selectivity. Compared with the  $C_{70}(OCH_3)_{10}$ , the UV-vis absorption and fluorescence of both the  $C_{70}(OCH_3)_{10}[C(COOEt)_2]$  and the  $C_{70}(OCH_3)_{10}[C(COOEt)_2]_2$  were blue-shifted due to the decrease in the  $\pi$ -conjugated system of the  $C_{70}$ . Moreover, the  $C_{70}(OCH_3)_{10}[C(COOEt)_2]$  and  $C_{70}(OCH_3)_{10}[C(COOEt)_2]_2$  showed blue fluorescence, and their fluorescence quantum yield was about ten times higher than that of the  $C_{70}(OCH_3)_{10}$ . The TD-DFT calculations indicated that the multi-functionalization of the  $C_{70}$  increased the  $S_1-T_1$  energy gap, reducing the intersystem crossing efficiency, resulting in the higher fluorescence quantum yield of the  $C_{70}$  derivatives. The results reveal that multi-functionalization is an effective strategy to improve the fluorescence of fullerene derivatives, providing novel organic electronic materials for organic light-emitting diodes.

**Supplementary Materials:** The following supporting information can be downloaded at: <https://www.mdpi.com/article/10.3390/nano12091426/s1>. Figure S1:  $^1H$  NMR spectrum (500 MHz,  $CDCl_3$ ) of  $C_{70}(OCH_3)_{10}[C(COOEt)_2]$ ; Figure S2:  $^{13}C$  NMR spectrum (500 MHz,  $CDCl_3$ ) of

$C_{70}(OCH_3)_{10}[C(COOEt)_2]$ ; Figure S3: ESI-FT-ICR-HRMS spectra of  $C_{70}(OCH_3)_{10}[C(COOEt)_2]$ ; Figure S4: COSY spectra of  $C_{70}(OCH_3)_{10}[C(COOEt)_2]$ ; Figure S5: HSQC of  $C_{70}(OCH_3)_{10}[C(COOEt)_2]$ ; Figure S6:  $^1H$  NMR spectrum (500 MHz,  $CDCl_3$ ) of  $C_{70}(OCH_3)_{10}[C(COOEt)_2]$ ; Figure S7:  $^{13}C$  NMR spectrum (500 MHz,  $CDCl_3$ ) of  $C_{70}(OCH_3)_{10}[C(COOEt)_2]$ ; Figure S8: ESI-FT-ICR-HRMS spectra of  $C_{70}(OCH_3)_{10}[C(COOEt)_2]$ ; Figure S9: COSY spectra of  $C_{70}(OCH_3)_{10}[C(COOEt)_2]$ ; Figure S10: HSQC spectra of  $C_{70}(OCH_3)_{10}[C(COOEt)_2]$ ; Table S1: Crystallographic data for  $C_{70}(OCH_3)_{10}[C(COOEt)_2]$ ; Figure S11: Natural Population Analysis (NPA) charge distribution of  $C_{70}(OCH_3)_{10}$  (A),  $C_{70}(OCH_3)_{10}[C(COOEt)_2]$ -I (B),  $C_{70}(OCH_3)_{10}[C(COOEt)_2]$ -II (C),  $C_{70}(OCH_3)_{10}[C(COOEt)_2]$ -III (D). And  $C_{70}(OCH_3)_{10}$  is shown in three orientations front view, top view and bottom view (E); Figure S12: Electrostatic potentials on the 0.001 a.u. molecular surfaces of  $C_{70}(OCH_3)_{10}$  (A),  $C_{70}(OCH_3)_{10}[C(COOEt)_2]$  (B) and  $C_{70}(OCH_3)_{10}[C(COOEt)_2]_2$  (C), calculated at B3LYP-D3BJ/6-31G(d, p) level with toluene solvent; Figure S13: Molecular orbitals (HOMO-1, HOMO, LUMO, and LUMO+1) of  $C_{70}(OCH_3)_{10}$  (A),  $C_{70}(OCH_3)_{10}[C(COOEt)_2]$  (B) and  $C_{70}(OCH_3)_{10}[C(COOEt)_2]_2$  (C) calculated at B3LYP-D3BJ/6-31G(d, p) level, in toluene; Figure S14: The most favorable structure of  $C_{70}(OCH_3)_{10}[C(COOEt)_2]_2$ . References [31–40] are cited in supplementary materials.

**Author Contributions:** Investigation, writing—original draft, K.L., L.W.; data collection, K.L., L.W., F.-F.X., B.-W.C. and Z.-C.C. Conceptualization, supervision, writing—revision, L.-L.D., S.-Y.X. and L.-S.Z. All authors have read and agreed to the published version of the manuscript.

**Funding:** This research was supported by the National Nature Science Foundation of China (21721001, 92061122, and 92061204).

**Data Availability Statement:** The data presented in this study are available in the article and Supplementary Materials.

**Conflicts of Interest:** The authors declare no conflict of interest.

## References

1. Negri, F.; Orlandi, G.; Zerbetto, F. Interpretation of the vibrational structure of the emission and absorption spectra of  $C_{60}$ . *J. Chem. Phys.* **1992**, *97*, 6496–6503. [[CrossRef](#)]
2. Van den Heuvel, D.J.; van den Berg, G.J.B.; Groenen, E.J.J.; Schmidt, J.; Holleman, I.; Meijer, G. Lowest Excited Singlet State of  $C_{60}$ : A Vibronic Analysis of the Fluorescence. *J. Phys. Chem.* **1995**, *99*, 11644–11649. [[CrossRef](#)]
3. Diehl, M.; Degen, J.; Schmidtke, H.-H. Vibronic structure and resonance effects in the optical spectra of the fullerenes  $C_{60}$  and  $C_{70}$ . *J. Phys. Chem.* **1995**, *99*, 10092–10096. [[CrossRef](#)]
4. Lin, S.-K.; Shiu, L.-L.; Chien, K.-M.; Luh, T.-Y.; Lin, T.-I. Fluorescence of fullerene derivatives at room temperature. *J. Phys. Chem.* **1995**, *99*, 105–111. [[CrossRef](#)]
5. Guldi, D.M.; Asmus, K.-D. Photophysical Properties of Mono- and Multiply-Functionalized Fullerene Derivatives. *J. Phys. Chem. A* **1997**, *101*, 1472–1481. [[CrossRef](#)]
6. Ma, B.; Bunker, C.E.; Guduru, R.; Zhang, X.-F.; Sun, Y.-P. Quantitative Spectroscopic Studies of the Photoexcited State Properties of Methano- and Pyrrolidino-[60]fullerene Derivatives. *J. Phys. Chem. A* **1997**, *101*, 5626–5632. [[CrossRef](#)]
7. Sun, Y.-P.; Lawson, G.E.; Riggs, J.E.; Ma, B.; Wang, N.; Moton, D.K. Photophysical and Nonlinear Optical Properties of [60]Fullerene Derivatives. *J. Phys. Chem. A* **1998**, *102*, 5520–5528. [[CrossRef](#)]
8. Sun, Y.-P.; Ma, B.; Bunker, C.E. Photoinduced Intramolecular  $n-\pi^*$  Electron Transfer in Aminofullerene Derivatives. *J. Phys. Chem. A* **1998**, *102*, 7580–7590. [[CrossRef](#)]
9. Williams, R.M.; Zwier, J.M.; Verhoeven, J.W. Photoinduced Intramolecular Electron Transfer in a Bridged  $C_{60}$  (Acceptor)-Aniline (Donor) System; Photophysical Properties of the First “Active” Fullerene Diad. *J. Am. Chem. Soc.* **1995**, *117*, 4093–4099. [[CrossRef](#)]
10. Guldi, D.M.; Prato, M. Excited-State Properties of  $C_{60}$  Fullerene Derivatives. *Acc. Chem. Res.* **2000**, *33*, 695–703. [[CrossRef](#)]
11. Giuffreda, M.G.; Negri, F.; Orlandi, G. Quantum-Chemical Modeling and Analysis of the Vibrational Structure in the Phosphorescence Spectrum of  $C_{60}$ . *J. Phys. Chem. A* **2001**, *105*, 9123–9129. [[CrossRef](#)]
12. Wang, L.; Liu, B.; Yu, S.; Yao, M.; Liu, D.; Hou, Y.; Cui, T.; Zou, G.; Sundqvist, B.; You, H.; et al. Highly Enhanced Luminescence from Single-Crystalline  $C_{60}$ -1m-xylene Nanorods. *Chem. Mater.* **2006**, *18*, 4190–4194. [[CrossRef](#)]
13. Accorsi, G.; Armaroli, N. Taking Advantage of the Electronic Excited States of [60]-Fullerenes. *J. Phys. Chem. C* **2010**, *114*, 1385–1403. [[CrossRef](#)]
14. Hutchison, K.; Gao, J.; Schick, G.; Rubin, Y.; Wudl, F. Bucky Light Bulbs: White Light Electroluminescence from a Fluorescent  $C_{60}$  Adduct—Single Layer Organic LED. *J. Am. Chem. Soc.* **1999**, *121*, 5611–5612. [[CrossRef](#)]
15. Matsuo, Y.; Sato, Y.; Hashiguchi, M.; Matsuo, K.; Nakamura, E. Synthesis, Electrochemical and Photophysical Properties, and Electroluminescent Performance of the Octa- and Deca(aryl)[60]fullerene Derivatives. *Adv. Funct. Mater.* **2009**, *19*, 2224–2229. [[CrossRef](#)]

16. Echegoyen, L.; Echegoyen, L.E. Electrochemistry of Fullerenes and Their Derivatives. *Acc. Chem. Res.* **1998**, *31*, 593–601. [[CrossRef](#)]
17. Hiroshi, I.; Kiyoshi, H.; Tsuyoshi, A.; Masanori, A.; Seiji, T.; Tadashi, O.; Masahiro, S.; Yoshiteru, S. The small reorganization energy of C<sub>60</sub> in electron transfer. *Chem. Phys. Lett.* **1996**, *263*, 545–550. [[CrossRef](#)]
18. Orlandi, G.; Negri, F. Electronic states and transitions in C<sub>60</sub> and C<sub>70</sub> fullerenes. *Photochem. Photobiol. Sci.* **2002**, *1*, 289–308. [[CrossRef](#)]
19. Arbogast, J.W.; Darmanyan, A.P.; Foote, C.S.; Diederich, F.N.; Whetten, R.L.; Rubin, Y.; Alvarez, M.M.; Anz, S.J. Photophysical properties of sixty atom carbon molecule (C<sub>60</sub>). *J. Phys. Chem.* **1991**, *95*, 11–12. [[CrossRef](#)]
20. Arbogast, J.W.; Foote, C.S. Photophysical properties of C<sub>70</sub>. *J. Am. Chem. Soc.* **1991**, *113*, 8886–8889. [[CrossRef](#)]
21. Kim, D.; Lee, M.; Suh, Y.D.; Kim, S.K. Observation of fluorescence emission from solutions of C<sub>60</sub> and C<sub>70</sub> fullerenes and measurement of their excited-state lifetimes. *J. Am. Chem. Soc.* **1992**, *114*, 4429–4430. [[CrossRef](#)]
22. Catalan, J.; Elguero, J. Fluorescence of fullerenes (C<sub>60</sub> and C<sub>70</sub>). *J. Am. Chem. Soc.* **1993**, *115*, 9249–9252. [[CrossRef](#)]
23. Li, Z.J.; Yang, W.W.; Gao, X. A room-temperature fluorescence study of organofullerenes: Cis-1 bisadduct with unusual blue-shifted emissions. *J. Phys. Chem. A* **2011**, *115*, 6432–6437. [[CrossRef](#)] [[PubMed](#)]
24. Schick, G.; Levitus, M.; Kvetko, L.; Johnson, B.A.; Lamparth, I.; Lunkwitz, R.; Ma, B.; Khan, S.I.; Garcia-Garibay, M.A.; Rubin, Y. Unusual Luminescence of Hexapyrrolidine Derivatives of C<sub>60</sub> with Th and Novel D3-Symmetry. *J. Am. Chem. Soc.* **1999**, *121*, 3246–3247. [[CrossRef](#)]
25. Li, C.Z.; Matsuo, Y.; Nakamura, E. Luminescent Bow-Tie-Shaped Decaaryl[60]fullerene Mesogens. *J. Am. Chem. Soc.* **2009**, *131*, 17058–17059. [[CrossRef](#)]
26. Matsuo, Y.; Tahara, K.; Morita, K.; Matsuo, K.; Nakamura, E. Regioselective eightfold and tenfold additions of a pyridine-modified organocopper reagent to [60]fullerene. *Angew. Chem. Int. Ed.* **2007**, *46*, 2844–2847. [[CrossRef](#)] [[PubMed](#)]
27. Fujita, T.; Matsuo, Y.; Nakamura, E. Synthesis of Tetradeca- and Pentadeca(organo)[60]fullerenes Containing Unique Photo- and Electroluminescent  $\pi$ -Conjugated Systems. *Chem. Mater.* **2012**, *24*, 3972–3980. [[CrossRef](#)]
28. Lou, N.; Li, Y.; Gan, L. Synthesis of C<sub>70</sub>-Based Fluorophores through Sequential Functionalization to Form Isomerically Pure Multiadducts. *Angew. Chem. Int. Ed.* **2017**, *56*, 2403–2407. [[CrossRef](#)]
29. Kornev, A.B.; Peregudov, A.S.; Martynenko, V.M.; Balzarini, J.; Hoorelbeke, B.; Troshin, P.A. Synthesis and antiviral activity of highly water-soluble polycarboxylic derivatives of [70]fullerene. *Chem. Commun.* **2011**, *47*, 8298–8300. [[CrossRef](#)]
30. Dolomanov, O.V.; Bourhis, L.J.; Gildea, R.J.; Howard, J.A.K.; Puschmann, H. OLEX2: A complete structure solution, refinement and analysis program. *J. Appl. Crystallogr.* **2009**, *42*, 339–341. [[CrossRef](#)]
31. Sheldrick, G.M. Crystal structure refinement with SHELXL. *Acta Crystallogr. Sect. C Struct. Chem.* **2015**, *71*, 3–8. [[CrossRef](#)] [[PubMed](#)]
32. Becke, A.D. Density-functional exchange-energy approximation with correct asymptotic behavior. *Phys. Rev. A* **1988**, *38*, 3098–3100. [[CrossRef](#)] [[PubMed](#)]
33. Becke, A.D. Density-functional thermochemistry. III. The role of exact exchange. *J. Chem. Phys.* **1993**, *98*, 5648–5652. [[CrossRef](#)]
34. Lee, C.; Yang, W.; Parr, R.G. Development of the Colle-Salvetti correlation-energy formula into a functional of the electron density. *Phys. Rev. B* **1988**, *37*, 785–789. [[CrossRef](#)]
35. Grimme, S.; Ehrlich, S.; Goerigk, L. Effect of the damping function in dispersion corrected density functional theory. *J. Comput. Chem.* **2011**, *32*, 1456–1465. [[CrossRef](#)]
36. Tomasi, J.; Mennucci, B.; Cammi, R. Quantum Mechanical Continuum Solvation Models. *Chem. Rev.* **2005**, *105*, 2999–3094. [[CrossRef](#)]
37. Humphrey, W.; Dalke, A.; Schulten, K. VMD: Visual molecular dynamics. *J. Mol. Graph.* **1996**, *14*, 33–38. [[CrossRef](#)]
38. Hirsch, A.; Lamparth, I.; Groesser, T.; Karfunkel, H.R. Regiochemistry of Multiple Additions to the Fullerene Core: Synthesis of a Th-Symmetric Hexakis adduct of C<sub>60</sub> with Bis(ethoxycarbonyl)methylene. *J. Am. Chem. Soc.* **1994**, *116*, 9385–9386. [[CrossRef](#)]
39. Guillot, S.; Chemelli, A.; Bhattacharyya, S.; Warmont, F.; Glatter, O. Ordered Structures in Carboxymethylcellulose–Cationic Surfactants–Copper Ions Precipitated Phases: In Situ Formation of Copper Nanoparticles. *J. Phys. Chem. B* **2009**, *113*, 15–23. [[CrossRef](#)]
40. Ovchinnikova, N.S.; Goryunkov, A.A.; Khavrel, P.A.; Belov, N.M.; Apenova, M.G.; Ioffe, I.N.; Yurovskaya, M.A.; Troyanov, S.I.; Sidorov, L.N.; Kemnitz, E. Unexpected fullerene dimerization via [5,6]-bond upon functionalization of Cs-C<sub>70</sub>(CF<sub>3</sub>)<sub>8</sub> by the Bingel reaction. *Dalton Trans.* **2011**, *40*, 959–965. [[CrossRef](#)]